# Effect of high SWNT content on the room temperature mechanical properties of fully dense 3YTZP/SWNT composites

R. Poyato*[,1], A. Gallardo-López[2], F. Gutiérrez-Mora[2], A. Morales-Rodríguez[2], A. Muñoz[2] y A. Domínguez-Rodríguez[2]

*1. Inst. Ciencia de Materiales de Sevilla (CSIC-Univ. Sevilla), Avda. Américo Vespucio 49, 41092 Sevilla*

*2. Dep. Física de la Materia Condensada, Univ. de Sevilla, apdo. 1065, 41012 Sevilla*

## Abstract

This paper is devoted to correlate the microstructure and room temperature mechanical properties of single-wall carbon nanotube (SWNT) reinforced 3 mol% yttria stabilized tetragonal zirconia with high SWNT content (2.5, 5 and 10 vol%). Fully dense composites were prepared by using a combination of aqueous colloidal powder processing and Spark Plasma Sintering. SWNTs were located at the ceramic grain boundaries and they were not damaged during the sintering process. The weak interfacial bonding between SWNTs and ceramic grains together with the detachment of SWNTs within thick bundles have been pointed out as responsible for the decrease of hardness and fracture toughness of the composites in comparison with the monolithic 3YTZP ceramic

**Keywords:** composites; carbon nanotubes; processing; Spark Plasma Sintering; mechanical properties

*Corresponding author. E-mail address: rosalia.poyato@icmse.csic.es

Phone number: +34 954 48 95 34

FAX number: +34 954 46 06 65

## 1. Introduction

During the last decade, there has been an increasing interest in the development of advanced ceramic matrix composites containing carbon nanotubes (CNTs)[1-3], as it is expected that some of the attractive properties of the CNTs[4,5] (high Young´s modulus, high tensile strength, high electrical conductivity or good thermal conductivity) will be transferred to the resulting composites. However, up to date, the positive effects of CNTs addition on the mechanical properties of ceramic matrix composites are still matter of debate. Whereas some groups reported enhancements in properties as fracture toughness or creep resistance[6-10], other authors found no improvements or even a detrimental effect of the CNTs addition[11-14].

The disparity of results can be related to the different processing methods used to prepare the composites, giving place to very different microstructures or not completely densified composites. The key points in the processing of these type of composites are, on one hand, a homogeneous dispersion of CNTs in the ceramic matrix together with a good interfacial bonding between both materials, and on the other, a high densification of the material. Several approaches, including different powder processing and sintering methods have been proposed in literature. Physical mixing under wet conditions by ultrasonication, ball milling or attrition milling has been conducted to disperse CNTs into alumina or zirconia powders[2,6,8-11]. Other approaches as colloidal processing including heterocoagulation, use of dispersants or charge stabilization have been also discussed in literature[13-17]. Recently, the in-situ growth of multi-wall carbon nanotubes (MWNT) onto alumina[18] or zirconia[19] particles was reported as a good approach to obtain a good dispersion of the CNTs in the ceramic matrix and a high density after consolidation by spark plasma sintering (SPS).

Among the published studies on ceramic matrix composites in recent years several works were devoted to the study of zirconia-based composites, as the superior mechanical properties and good ionic conductivity of yttria-doped zirconia make this ceramic a technologically interesting material for a wide range of applications such as structural material, solid oxide fuel cells or oxygen sensors[20-22].

Most of the studies about CNTs reinforced zirconia reported heterocoagulation or use of dispersants for the processing of the composite powder[13-15,23,24], sometimes combined with other techniques such as slip-casting[14] or spray drying[25]. Regarding the densification step, hot pressing[13,25] or conventional[14] sintering were used by some authors. Garmendia *et al*[14] reported a colloidal processing route based on the strong attractive interaction of the MWNT and the 3 mol% yttria-doped zirconia (3YTZP) powder by heterocoagulation, using poly(ethylenimine) (PEI) as cationic dispersant. After slip casting and conventional sintering they obtained composites with 96% of the theoretical density. In their study, significant improvements in hardness or fracture toughness were not achieved. Zhou *et al*[25] combined heterocoagulation using polyacrylate acid (PAA) with spray drying to obtain the 3YTZP/MWNT composite powder. Fully densified composites were not obtained after hot-pressing the composites (98% of the theoretical density for composites with 0.5 and 1 wt% MWNT). However, increases in flexural strength and fracture toughness were reported up to 1.0 wt% MWNT.

Among the reported studies on CNT/3YTZP composites, highly densified samples were only obtained in studies using SPS[19,23,24]. Nevertheless, a decrease of hardness in the composites when compared with the monolithic ceramic, even when they are fully densified, and an increase of fracture toughness only for low percentages of CNTs[11,15,19,23-25] have been reported in most of these studies. Recently, Mazaheri *et*

*al*[8,9] reported an increase of fracture toughness on nearly fully dense 3 mol% yttria-doped zirconia reinforced with 0.5-5 wt% MWNT with no detrimental effect on hardness. These composites were prepared by a combination of attrition milling and SPS.

Up to date, most of the investigations focused on MWNT reinforced yttria-doped zirconia, however, the study of processing and mechanical properties of single wall carbon nanotube (SWNT) reinforced yttria stabilized zirconia composites is still a challenge. SWNT present better mechanical properties than MWNT as it is possible to avoid the inter-wall sliding that can take place in MWNT, with inner graphitic walls being extracted from outer walls in a "sword and sheath" failure[6,26]. However, SWNT tend to agglomerate easily due to Van der Waals interactions, which complicate the composites processing. Recently, Shin and Hong[27] reported on the processing and microstructure of SWNT reinforced yttria stabilized zirconia composites with promising mechanical and tribological properties. These authors combined the use of dimethylformamide as a solvent to disperse the SWNT in the matrix with SPS to obtain composites with 0.1-1.0 wt% SWNT. Although full densification was not obtained in the whole set of composites, an enhancement of fracture toughness together with an improvement of wear properties was reported.

In recent years, an intense debate on the reliability of different fracture toughness measurement methods to characterize CNT-ceramic matrix composites has taken place[12,23,28-31]. There have been different arguments about the validity of the indentation technique, and some authors have compared the results obtained using this method with the ones obtained with the single edge notched beam (SENB) test. Wang e*t al*[12] have shown that cracks are hardly produced in SWNT-$Al_2O_3$ composites after Vickers or Hertzian indentation, which would give extremely high fracture toughness

values; however, no increase of fracture toughness was obtained from SENB measurements. An increase of $K_{IC}$ when increasing the CNT content has been reported by Cho *et al*[31] and Mazaheri *et al*[9] for MWNT-$SiO_2$ and MWNT-3YTZP composites, respectively. Although the absolute values of $K_{IC}$ measured by Vickers indentation or SENB test differ (higher values obtained from indentation measurements), a similar trend was observed when measuring using the two techniques. It seems clear that the indentation technique should not be used to determine absolute values of $K_{IC}$ in CNT-ceramic matrix composites. Nevertheless, it has been proposed that this test could be useful for assessing relative toughness values in well-densified materials with good nanoscale dispersion if sufficiently developed cracks are produced[23,31]. In this context, although the $K_{IC}$ values obtained from Vickers indentations are not directly comparable to values in the literature for materials tested with the SENB method, they can be used to compare different compositions tested in a same study.

In this work, 3 mol% yttria doped zirconia matrix composites containing high SWNT content (2.5, 5 and 10 vol%) were prepared by using a combination of aqueous colloidal processing and Spark Plasma Sintering. Full densification, together with homogeneous dispersion of the SWNT throughout the ceramic matrix in the nanoscale, was obtained. The microstructure of the composites was characterized and the evolution of their hardness and fracture toughness with SWNT volume fraction was analysed.

## 2. Experimental procedure

### 2.1. Materials Processing

#### *2.1.1 SWNTs acid treatment*

Commercially available purified SWNT (Carbon Solutions Inc., Riverside, California) were selected as starting material. Acid treatment of the SWNTs was carried out using a mixture of concentrated sulfuric acid (98%) and nitric acid (70%) in the ratio 3:1, with the aim of disentangle and cut the raw SWNTs ropes[16,32]. SWNTs were suspended in the acid mixture for 24 h at room temperature; the suspension was sonicated for 8 h. SWNTs were collected on ~20 nm pore filter membranes and washed with high-purity ethanol several times. The acid-treated SWNTs were then dried on hot plate at 70-80 ºC and homogenized in agate mortar.

*2.1.2 3YTZP-SWNTs powder colloidal processing*

3 mol% yttria stabilized tetragonal zirconia powder (3YTZP), with 40 nm particle size and 99% purity, was obtained from a commercial source (Nanostructured and Amorphous Materials Inc., Houston, Texas). Colloidal processing[16] of the composite powders (2.5, 5 and 10 vol% SWNTs) was carried out in aqueous solution of pH 12, where both the SWNTs and the 3YTZP nanoparticle surfaces are negatively charged, using $NH_3$ to adjust the solution pH. In a first step, independent SWNTs and ceramic powder solutions were prepared and subjected to ultrasonic agitation for 30 min. In a second step, 3YTZP+SWNTs powder blends were dispersed in aqueous solution and subjected to ultrasonic agitation for 30 min, followed by drying on a hot plate while being stirred. Finally, composite powders were homogenized in agate mortar.

By using this colloidal dispersion by charge stabilization we avoid using surfactants that could introduce undesirable impurities which could affect the sintering process and/or composites properties.

*2.1.3 Spark Plasma Sintering (SPS)*

The SPS (Model 515S, SPS Dr Sinter Inc., Kanagawa, Japan) of the composite powders was performed in vacuum in a 15-mm diameter cylindrical graphite die/punch setup, under a uniaxial pressure of 75 MPa at 1250 °C for 5 min. The heating and cooling rates were 300 and 50 °C/min, respectively. For the sake of comparison, monolithic 3YTZP ceramic was sintered using the same conditions. A sheet of graphite paper was placed between the powders and die/punches for easy specimen removal. Temperature was measured by means of an optical pyrometer focused on a bore hole in the middle part of the graphite die. The sintered ceramics of ~15 mm in diameter and ~2 mm in thickness were ground to eliminate the surface carbon.

Density of the composites was determined using the Archimedes' method, using water as the immersion liquid. The theoretical densities of the composites were calculated according to the rule of the mixtures, assuming a density of 1.80 g $cm^{-3}$ for SWNTs[3].

## 2.2. Microstructural and mechanical characterization

Phase identification was carried out using X-ray diffraction (XRD, model D8 Advance A25, Bruker Co., Massachusetts, USA). The Rietveld method was used for quantitative analysis using the FULLPROF program.

Sintered composites were characterized by Raman spectroscopy in order to detect possible damage of SWNTs after sintering. Raman spectra were recorded on fracture surfaces using a dispersive microscope (Horiba Jobin Yvon LabRam HR800, Kyoto, Japan), with a 20-mW He-Ne green laser (532.14 nm), without filter, and with a

600 g/mm grating. The microscope used a 100x objective and a confocal pinhole of 100 μm. The Raman spectrometer was calibrated using a silicon wafer.

Microstructural observations of sintered composites were carried out on the fracture and polished surfaces by high-resolution scanning electron microscopy (HRSEM), using a Hitachi S5200 microscope (Hitachi High Technologies America Inc., USA). Polished samples (up to 1 μm diamond paste) were thermally etched at 1150 ºC for 20 min in air to reveal the grain boundaries. The morphological parameters equivalent planar diameter, $d = (4\times\text{area}/\pi)^{1/2}$ and shape factor, $F = (\text{perimeter})^2/4\times\text{area}$, were measured on HRSEM micrographs by using ImageJ software.

Vickers indentation tests were carried out with a diamond Vickers indenter to establish the hardness and fracture toughness at room temperature, under 2 kgf and 10 kgf, respectively. At least 15 valid measurements were carried out on mirror-like finished top surfaces for each sample, in well-separated and randomly selected regions. The crack lengths were measured using a LEICA DCM 3D confocal microscope.

The fracture toughness, $K_{IC}$, was calculated by using the equation given by Anstis *et al.*[33] .

$$K_{IC} = 0.016\left(\frac{E}{H}\right)^{1/2}\left(\frac{P}{c^{3/2}}\right) \quad (1)$$

where $c$ is the crack length measured from the center of the imprint, $E$ is the elastic modulus in GPa and $H$ is the Vickers hardness in GPa, calculated from the indentation load $P$ and the diagonal of the Vickers imprint $a$:

$$H = 1.854\frac{P}{a^2} \quad (2)$$

## 3. Results and discussion

Figure 1 shows the evolution of the shrinkage and temperature as a function of time during heating and stabilization at the sintering temperature for the composites with different SWNTs content. This evolution was recorded *in situ* during the SPS process. It can be observed that sintering takes place mainly for temperatures higher than 850 ºC and up to 1200 ºC, with a slight density enhancement for temperatures from 1200 ºC to 1250 ºC. A similar behaviour is observed in all sintered composites, which is in agreement with the full densification measured by the Archimedes method in the three composites **(>99% relative density for the three composites, table 1)**.

XRD patterns of the sintered specimens are shown in figure 2. In all the samples, it is clear the presence of the tetragonal phase (JCPDS 01-078-1808) as the main one, with a contribution of the monoclinic phase (JCPDS 01-081-1314). Rietveld refinement carried out for the monolithic 3YTZP ceramic pointed out the formation of these two phases, being the major crystalline phase the tetragonal one (92.4%) and the minor phase the monoclinic one (7.6%). An increase of the two main peaks corresponding to the monoclinic phase (at 28.2 and 31.4 º2θ) is clearly observed when increasing the SWNT content. Thus, the transformation of the tetragonal phase to the monoclinic one is clearly favoured by the addition of SWNT. Bocanegra-Bernal *et al*[34] have recently experimentally evidenced such transformation in $ZrO_2$ for zirconia toughened alumina (ZTA)/0.01 wt% MWNT composites pressureless sintered in air using graphite as bed powder. The increasing effect observed in our results states that it is indeed the presence of carbon nanotubes (SWNTs in this case) which promotes the presence of the monoclinic phase. However, the mechanism of this transformation is still unclear and future work on this subject will be carried out.

Figure 3 shows the Raman spectra measured in the sintered composites, as well as in the monolithic 3YTZP ceramic and in the SWNTs. The Raman spectra measured

in the composites show characteristic radial breathing mode (RBM) bands near 150–200 $cm^{-1}$ and G-bands near 1500–1600 $cm^{-1}$, which are very similar to the measured ones in the SWNT before processing of the composites. These results clearly demonstrate the presence of SWNTs after SPS. The D-band (centred on 1350 $cm^{-1}$) shows a slight increase, which can be attributed to the formation of disordered graphite and defects in the composites during the SPS process. When comparing the spectra measured in the composites and in the SWNTs, a shift towards higher frequencies is observed in the composites G-band (~20 $cm^{-1}$), which has been attributed by different authors to residual stresses in the SWNTs imposed by the constraining ceramic matrix[12,35]. On the other hand, peaks at 165, 260, 320, 465, 610, and 643 $cm^{-1}$ are observed in the spectra measured in the composites. These peaks correspond to the six Raman bands predicted for theoretical tetragonal zirconia, as has been described by previous authors[36,37].

HR-SEM micrographs of fracture surface of the composites reinforced with different SWNTs content are presented in figure 4. SWNTs bundles are located on the ceramic grain boundaries and debonded CNTs from the matrix can be observed on the fracture surfaces. The fracture mode is mainly intergranular (grain boundary weakness due to the presence of the SWNTs promotes intergranular fracture along grain boundaries, over transgranular fracture through the grains). SWNTs are well distributed on the ceramic matrix, however, some agglomerates could be observed in the composites (not shown). The presence of these nanotube agglomerates or clusters has been reported by previous authors[10,13,17,23,25]. Recently, Poorteman *et al*[17] found such inhomogeneities in MWNT-ceramic matrix composites even after using aqueous colloidal processing optimizing electrostatic repulsion and conserving the homogeneity by freeze-drying the composite powder. A thermodynamic explanation based on the free

volume of isotropic particles and particles with a high aspect ratio, which promotes the demixion of both phases, was suggested.

Figure 5 shows the HR-SEM micrographs of thermally etched polished surfaces and grain size distribution plots of monolithic 3YTZP ceramic and composite with 5 vol% SWNTs. An equiaxed grain microstructure was found in all the materials (shape factor around 0.8, table 1). Some holes can be observed (fig. 5(c)), which could correspond to previous locations of SWNT bundles or agglomerates burned out during thermal etching in air. While global microstructure presents a mean grain size about 250 nm for all compositions (table 1), areas with larger grain sizes were scarcely observed (not shown). These zones could be related to monoclinic transformed regions.

Some authors have reported a decrease in grain size with increasing SWNT content, however, this reduction is usually related to a decrease in the density of the composite[10,13,27]. This fact can be ruled out in this study, since all the processed composites are fully densified and a clear effect of the SWNT percentage on the mean grain size is not observed (table 1).

Regarding the room-temperature mechanical properties, a decrease in Vickers hardness is found when increasing the SWNTs content (figure 6). The same behaviour has been recently reported in fully densified MWNT-3YTZP composites[23,24]. Although this tendency is usually linked to a decrease in the composite density[13,25,27], the SWNT-3YTZP composites studied in this work are fully densified, denoting the decrease in hardness when increasing the CNTs content as an intrinsic effect of the CNT-3YTZP system probably associated to weak interfacial bonding between SWNTs and ceramic grains.

SEM micrographs of the Vickers indentations performed in the studied composites are shown in figure 7. Values of fracture toughness obtained from these

measurements as a function of SWNT content are shown in figure 6. Lower fracture toughness is obtained for the composites when compared to monolithic ceramic. On the other hand, no significant effect of the difference in SWNT content on the fracture toughness value is observed. This result is in disagreement with the increase of fracture toughness in SWNT-3YTZP composites recently reported by Shin and Hong[27]. However, it should be noted that these authors used lower SWNT content (up to 1.0 wt %) than the ones used in the present study (up to 10 vol %) to reinforce the 3YTZP ceramic matrix. A similar reinforcing effect has been reported also in MWNT-3YTZP composites, with an increase of fracture toughness for low CNT contents followed by a decrease for high CNT contents[11,15,23,25]. **A comparative of the relative toughness variation reported in literature for different CNT-3YTZP composites, according to the type and CNT content used, relative density and zirconia grain size, is shown in table 2.**

Some authors have reported that large quantities of SWNTs would impede the densification process, leading to possible residual porosity and a subsequent decrease in mechanical properties[13,25,27]. Also, it is widely accepted that polycrystalline tetragonal zirconia compositions exhibit a substantial decrease in the contribution of transformation toughening to the fracture toughness with decrease in grain size[38]. However, the decrease of fracture toughness in the composites under study can not be related to factors as possible residual porosity or smaller mean grain size with respect to the monolithic ceramic, as it has been shown that all the processed samples are fully dense and no significant differences were detected in grain size between the monolithic ceramic and the composites (Table 1).

The classical toughening mechanisms described for conventional ceramic composites reinforced by fibers or whiskers, such as fiber pull-out, crack deflection and

crack bridging, have been mentioned in literature as useful to describe toughening in CNT-ceramic matrix composites[10,39,40]. However, another possible mechanism based in uncoiling and stretching of CNTs has been recently described as responsible of enhanced toughness in these composites[2,9]. What appears to occur in this mechanism is the uncoiling of the CNTs bundles located at the ceramic grain boundaries in the crack wake as the crack advances intergranularly. With further propagation of the crack, the uncoiled CNTs would stretch, producing crack bridging. The uncoiling and stretching produces friction work and dissipates energy at the crack tip, resulting in higher toughness[2,9].

In the SEM micrographs of the 3YTZP/5 vol% SWNTs composite fracture surface, SWNT bridging between ceramic grains could be found (figure 4d). SWNTs with two ends embedded in two separate grains are clearly observed. This observation is in line with previous findings in CNT ceramic and glass composites[9,23-25,40]. However, these SWNT bridging were scarcely found in our composites.

Considering that evidences of toughening mechanisms have not been detected and taking into account that the SWNT volume fraction used in this study is higher than the ones used by other authors[27], it could be concluded that the SWNT amounts used in this study exceed the appropriate percentages that would result in an enhancement of fracture toughness.

Using the model developed by Zapata-Solvas et al[41], it is possible to calculate the surface fraction of ceramic grains in contact with SWNTs, *A*, for the values of studied SWNT volume fractions according to:

$$A = \frac{f(1-f)d}{4w} \qquad (3)$$

Considering an estimated mean SWNT bundle diameter *w* of about 25 nm[42] and mean grain size *d* ~250 nm, we obtain that 22, 12 and 6% of surface fraction of ceramic grains are covered by SWNTs for compositions with 10, 5 and 2.5 vol% SWNTs, respectively. Those percentages are clearly above percolation[41]. Also, this calculation reveals that the processing route used to prepare the composites gives place to a low coverage of the ceramic grains due to the existence of thick SWNT bundles (about 15 SWNTs each), which would result in a poor reinforcing effect in any case.

The accumulation of SWNT at the grain boundaries in form of thick bundles would not allow the uncoiling and stretching of SWNT when the crack is advancing but it would result in a decrease in cohesion between ceramic grains. Moreover, inter bundles detachment would be favoured rather than uncoiling and stretching, being the decohesion between SWNT within the bundle the key point in the process. 3 point bending tests carried out in SWNT solids[43] revealed that failure occurred via inter-bundles slippage rather than the failure of the SWNTs themselves.

Taking into account the mechanism proposed above, the fact that the SWNT contents in our composites are higher than the percolation limit would explain that the fracture toughness values are independent of the SWNT vol%.

Future work will be performed to clarify whether a toughness enhancement mechanism exists in low SWNT content composites, in order to assess if lower SWNT vol% results in thinner SWNT bundles surrounding the ceramic grains and that finally results in an enhancement of the mechanical properties of the composite.

## 4. Conclusions

Fully dense 3 mol% yttria doped zirconia matrix composites containing 2.5, 5 and 10 vol% SWNT have been prepared by using a combination of aqueous colloidal powder processing and Spark Plasma Sintering. All the samples are mainly tetragonal, with a minor contribution of the monoclinic phase. An increase of the latter when increasing the SWNT content was found, pointing to a transformation of the tetragonal phase to the monoclinic one promoted by the presence of SWNTs.

An equiaxed grain microstructure and an almost constant ceramic grain size (190-270 nm) have been obtained in the composites. SWNTs were located on the ceramic grain boundaries and homogeneously distributed on the ceramic matrix at the nanoscale, however, the presence of large SWNT agglomerates could not be avoided.

A decrease in hardness has been found when increasing the SWNTs content in spite of the full densification of the composites. A decrease of the fracture toughness was also found, possibly as a consequence of a SWNT weakening effect on interfacial cohesion between ceramic grains. The detachment between SWNT within bundles has been pointed out as the decisive point in the fracture process.

**Acknowledgements**

The financial support for this work has been obtained from the Spanish Ministry of Science and Innovation (MAT2012-34217) and from Junta de Andalucía (P12-FQM-1079). XRD and microscopy studies have been performed in facilities belonging to the CITIUS (Universidad de Sevilla). Prof. F.L. Cumbrera (Univ. of Sevilla) is greatly acknowledged for the Rietveld refinement.

**References**


[1] J. Cho, A.R. Boccaccini, M.S.P. Shaffer, Ceramic matrix composites containing carbon nanotubes, J. Mater. Sci. 44 (2009) 1934-51.

[2] N.P. Padture, Multifunctional composites of ceramics and single-walled Carbon nanotubes, Adv. Mater. 21 (2009) 1767–70.

[3] P.J.F. Harris, Carbon nanotube composites, Int. Mater. Rev. 49 (2004) 31-43.

[4] S. Iijima, C.H. Brabec, A. Maiti, Z.J. Bernholc, Structural flexibility of carbon nanotubes, J. Chem. Phys. 104 (1996) 2089–92.

[5] R.H. Baughman, A.A. Zakhidov, W.A. Heer, Carbon nanotubes- The route toward applications, Science 297 (2002) 787–92.

[6] G.D. Zhan, J.D. Kuntz, J. Wan, A.K. Mukherjee, Single-wall carbon nanotubes as attractive toughening agents in alumina based nanocomposites, Nat. Mater. 2 (2003) 38-42.

[7] E. Zapata-Solvas, R. Poyato, D. Gómez-García, A. Domínguez-Rodríguez, V. Radmilovic, N.P. Padture, Creep-resistant composites of alumina and single-wall carbon nanotubes, Appl. Phys. Lett. 92 (2008) 111912.

[8] M. Mazaheri, D. Mari, R. Schaller, G. Bonnefont, G. Fantozzi, Processing of yttria stabilized zirconia reinforced with multi-walled carbon nanotubes with attractive mechanical properties, J. Eur. Ceram. Soc. 31 (2011) 2691-98.

[9] M. Mazaheri, D. Mari, Z. Razavi Hesabi, R. Schaller, G. Fantozzi, Multi-walled carbon nanotube/nanostructured zirconia composites: Outstanding mechanical properties in a wide range of temperature, Composites Sci. Technol. 71 (2011) 939-45.

[10] I. Ahmad, H. Cao, H. Chen, H. Zhao, A. Kennedy, Y.Q. Zhu, Carbon nanotube toughened aluminum oxide nanocomposite, J. Eur. Ceram. Soc. 30 (2010) 865-873.

[11] T. Ukai, T. Sekino, A. Hirvonen, N. Tanaka, T. Kusunose, T. Nakayama, K. Niihara, Preparation and electrical properties of carbon nanotubes dispersed zirconia nanocomposites, Key Eng. Mater. 317-318 (2006) 661-64.

[12] X. Wang, N.P. Padture, H. Tanaka, Contact-damage-resistant ceramic/single-wall carbon nanotubes and ceramic/graphite composites, Nat. Mater. 3 (2004) 539-44.

[13] A. Duszová, J. Dusza, K. Tomasek, G. Blugan, J. Kuebler, Microstructure and properties of carbon nanotube/zirconia composite, J. Eur. Ceram. Soc. 28 (2008) 1023-27.

[14] N. Garmendia, I. Santacruz, R. Moreno, I. Obieta, Slip casting of nanozirconia/MWCNTcomposites using a heterocoagulation process, J. Eur. Ceram. Soc. 29 (2009) 1939-45.

[15] J. Sun, L. Gao, M. Iwasa, T. Nakayama, K. Niihara, Failure investigation of carbon nanotube/3Y-TZP nanocomposites, Ceram. Int. 31 (2005) 1131–1134.

[16] R. Poyato, A.L. Vasiliev, N.P. Padture, H. Tanaka, T. Nishimura, Aqueous colloidal processing of single-wall carbon nanotubes and their composites with ceramics, Nanotech. 17 (2006) 1770–1777.

[17] M. Poorteman, M. Traianidis, G. Bister, F. Cambier, Colloidal processing, hot pressing and characterisation of electroconductive MWCNT-alumina composites with compositions near the percolation threshold, J. Eur. Ceram. Soc. 29 (2009) 669-675.

[18] T. Zhang, L. Kumari, G.H. Du, W.Z. Li, Q.W. Wang, K. Balani, A. Agarwal, Mechanical properties of carbon nanotube–alumina nanocomposites synthesized by chemical vapor deposition and spark plasma sintering, Compos: Part A 40 (2009) 86–93.

[19] A. Datye, K.H. Wu, G. Gomes, V. Monroy, H.T. Lin, J. Vleugels, K. Vanmeensel, Synthesis, microstructure and mechanical properties of yttria stabbilized zirconia

(3YTZP)-multi-walled nanotube (MWNTs) nanocomposite by direct in-situ growth of MWNTs on zirconia particles, Composites Sci. Technol. 70 (2010) 2086-92.

[20] N.Q. Minh, Ceramic fuel cells, J. Am. Ceram. Soc. 76 (1993) 563–588.

[21] W.C. Maskell, Progress in the development of zirconia gas sensors, Solid State Ion. 134 (2000) 43-50.

[22] S. Deville, L. Gremillard, J. Chevalier, G. Fantozzi, A critical comparison of methods for the determination of the aging sensitivity in biomedical grade yttria-stabilized zirconia, J. Biomed. Mater. Res. B: Appl. Biomater. 72 (2005) 239-45.

[23] N. Garmendia, S. Grandjean, J. Chevalier, L.A. Diaz, R. Torrecillas, I. Objeta, Zirconia-multiwall carbon nanotubes dense nano-composites with an inusual balance between crack and ageing resistance, J. Eur. Ceram. Soc. 31 (2011) 1009-14.

[24] R.K. Chintapalli, F. Garcia Marro, B. Milsom, M. Reece, M. Anglada, Processing and characterization of high-density zirconia-carbon nanotube composites, Mater. Sci. Eng. A 549 (2012) 50-59.

[25] J.P. Zhou, Q.M. Gong, K.Y. Yuan, J.J. Wu, Y.F. Chen, C.S. Li, J. Liang, The effects of multiwalled carbon nanotubes on the hot-pressed 3 mol% yttria stabilized zirconia ceramics, Mater. Sci. Eng. A 520 (2009) 153-57.

[26] M.H. Bocanegra-Bernal, J. Echeberria, J. Ollo, A. Garcia-Reyes, Domínguez-Rios, A. Reyes-Rojas, A. Aguilar-Elguezabal, A comparison of the effects of multi-wall and single-wall carbon nanotube additions on the properties of zirconia toughened alumina composites, Carbon 49 (2011) 1599-1607.

[27] J.H. Shin, S.H. Hong, Microstructure and mechanical properties of single wall carbon nanotube reinforced yttria stabilized zircona ceramics, Mater. Sci. Eng. A 556 (2012) 382-87.

[28] D. Jiang, K. Thomson, J.D. Kuntz, J.W. Ager, A.K. Mukherjee, Effect of sintering temperature on a single-wall carbon nanotube-toughened alumina-based nanocomposite, Scripta Mater. 56 (2007) 959-62.

[29] N.P. Padture, W.A. Curtin, Comment on "Effect of sintering temperature on a single-wall carbon nanotube-toughened alumina-based nanocomposite", Scripta Mater. 58 (2008) 989-90.

[30] D. Jiang, A.K. Mukherjee, Response to comment on "Effect of sintering temperature on a single-wall carbon nanotube-toughened alumina-based nanocomposite", Scripta Mater. 58 (2008) 991-93.

[31] J. Cho, F. Inam, M.J. Reece, Z. Chlup, I. Dlouhy, M.S.P. Shaffer, A.R. Boccaccini, Carbon nanotubes: do they toughen brittle matrices?, J. Mater. Sci. 46 (2011) 4770-79.

[32] J. Liu, A.G. Rinzler, H. Dai, J.H. Hafner, R.K. Bradley, P.J. Boul, A. Lu, T. Iverson, K. Shelimov, C.B. Huffman, F. Rodríguez-Macías, Y.S. Shon, T.R. Lee, D.T. Colbert, R.E. Smalley, Fullerene Pipes, Science 280 (1998) 1253-56.

[33] G.R. Anstis, P. Chantikul, D.B. Lawn, D.B. Marshall, A critical evaluation of indentation techniques for measuring fracture toughness: I. direct crack measurement, J. Am. Ceram. Soc. 64 (1981) 533–38.

[34] M.H. Bocanegra-Bernal, A. Reyes-Rojas, A. Aguilar-Elguezabal, E. Torres-Moye, J. Echeberria, X-ray diffraction evidence of a phase transformation in zirconia by the presence of graphite and carbon nanotubes in zirconia toughened alumina composites, Int. J. Ref. Metals Hard Mater. 35 (2012) 315-18.

[35] P.M. Ajayan, L.S. Schadler, C. Giannaris, A. Rubio, Single-walled carbon nanotube-polymer composites: Strength and weakness, Adv. Mater. 12 (2000) 750–3.

[36] M. Li, Z. Feng, G. Xiang, P. Ying, Q. Xin, C. Li, Phase Transformation in the Surface Region of Zirconia Detected by UV Raman Spectroscopy, J. Phys. Chem. B 105 (2001) 8107–11.

[37] S.A. Cruz, R. Poyato, F.L. Cumbrera, J.A. Odriozola, Nanostructured Spark Plasma Sintered Ce-TZP Ceramics, J. Am. Ceram. Soc. 95 (2012) 901–906.

[38] P.F. Bechar and M.V. Swain, Grain-size-dependent transformation behaviour in polycrystalline tetragonal zirconia, J. Am. Ceram. Soc. 75 (1992) 493-502.

[39] Z. Xia, L. Riester, W.A. Curtin, H. Li, B.W. Sheldon, J. Liang, B. Chang, J.M. Xu, Direct observation of toughening mechanisms in carbon nanotube ceramic matrix composites, Acta Mater. 52 (2004) 931–44.

[40] A. Mukhopadhyay, B.T.T. Chu, M.L.H. Green, R.I. Todd, Understanding the mechanical reinforcement of uniformly dispersed multiwalled carbon nanotubes in alumino-borosilicate glass ceramic, Acta Mater. 58 (2010) 2685–97.

[41] E. Zapata-Solvas, D. Gómez-García, A. Domínguez-Rodríguez, On the microstructure of single wall carbon nanotubes reinforced ceramic matrix composites, J. Mater. Sci. 45 (2012) 2258-63.

[42] E. Zapata-Solvas, D. Gómez-García, A. Domínguez-Rodríguez, Towards physical properties tailoring of carbon nanotubes-reinforced caremic matrix composites, J. Eur. Ceram. Soc. 32 (2012) 3001-3020.

[43] G. Yamamoto, Y. Sato, T. Takahashi, M. Omori, T. Hashida, A. Okubo, K. Tohji, Single-walled carbon nanotube-derived novel structural material, J. Mater. Res. 21 (2006) 1537-1542.

**Figure captions**

**Figure 1**: Shrinkage and temperature curves recorded during the SPS processing of the 3YTZP/SWNTs composites.

**Figure 2**: X-ray diffraction patterns of the monolithic 3YTZP ceramic and the composites.

**Figure 3**: Raman spectra measured in the composites including the RBM frequency range, and the D-Band and G-Band frequency range. Raman spectra measured in the monolithic 3YTZP ceramic and in the SWNTs have been included for comparison.

**Figure 4**: HRSEM micrographs of fracture surface of the composites reinforced with different SWNT contents (a) and (b) 2.5 vol%, (c) and (d) 5 vol%, and (e) and (f) 10 vol%.

**Figure 5**: HRSEM micrographs of thermally etched polished surfaces and grain size distribution plots of the (a) monolithic 3YTZP ceramic, and (b) composite reinforced with 5 vol% SWNTs. (c) HRSEM micrographs of thermally etched polished surface of the 3YTZP/5 vol% SWNTs composite, showing some holes related to agglomerates burned out during thermal etching in air.

**Figure 6**: Hardness and indentation fracture toughness of the SWNT-3YTZP composites.

*Corresponding author. E-mail address: rosalia.poyato@icmse.csic.es
Phone number: +34 954 48 95 34
FAX number: +34 954 46 06 65

**Figure 7**: SEM micrographs of the Vickers indentations in the composites with (a) 2.5, (b) 5, and (c) 10 vol% SWNTs.

**Table 1**: Properties of the studied composites

| Material | Relative density (%) | Grain size (μm) | F | Hardness (GPa) | Fracture toughness ($MPa \cdot m^{1/2}$) |
|---|---|---|---|---|---|
| **3YTZP** | **100** | 0.26 ± 0.11 | 0.76 ± 0.06 | 13.0 ± 0.5 | 6.1 ± 0.9 |
| **3YTZP/2.5 vol% SWNT** | **100** | 0.27 ± 0.13 | 0.76 ± 0.06 | 12.4 ± 0.7 | 4.7 ± 0.9 |
| **3YTZP/5 vol% SWNT** | **99.3** | 0.19 ± 0.08 | 0.76 ± 0.07 | 11.4 ± 0.5 | 4.8 ± 0.6 |
| **3YTZP/10 vol% SWNT** | **100** | 0.24 ± 0.13 | 0.76 ± 0.08 | 9.2 ± 0.9 | 5.0 ± 0.8 |

**Table 2: Comparison of properties for CNT-3YTZP composites reported in literature.**

| | Type of CNT | CNT vol% | Grain size (nm) | Relative Density (%) | Method of $K_{IC}$ measurement | $K_{IC}$ (MPa·m$^{1/2}$) | | Relative $K_{IC}$ variation (%) |
|---|---|---|---|---|---|---|---|---|
| | | | | | | Monolithic | Composite | |
| This study | SWNT | 2.5 | 270 | 100 | IF | 6.1 | 4.7 | -23 |
| Shin 2012 (27) | SWNT | 3.4 | 280 | 98.0 | IF | 4.4 | 5.2 | 18 |
| Chintapalli 2012 (24) | MWNT | 2 | 161 | 98.7 | IF | 3.9 | 4.5 | 15 |
| Garmendia 2011 (23) | MWNT | 3 | 218 | 99.5 | IF | 2.36 | 4.06 | 72 |
| | | 6 | 146 | 99.1 | IF | 2.36 | 2.07 | -14 |
| Mazaheri 2011 (9) | MWNT | 12.5 | 96 | 98.4 | IF | 5.5 | 11 | 100 |
| | | | | | SENB | 6 | 8 | 33 |
| Zhou 2009 (25) | MWNT | 3.4 | --- | 98.6 | IF | 4.9 | 5.8 | 21 |
| | | 5 | --- | 98 | IF | 4.9 | 5.2 | 5 |
| Garmendia 2009 | MWNT | 1 | 220 | 95.7 | IF | 3.8 | 4.0 | 5 |
| Duszová 2008 (13) | MWNT | 3.4 | 140 | 88 | IF | 6.24 | 5.6 | -10 |
| Ukai 2006 (11) | MWNT | 1.7 | --- | 100 | IF | 5.56 | 6.10 | 10 |
| | | 3.4 | --- | 100 | IF | 5.56 | 5.69 | 2 |
| Sun 2005 (15) | MWNT | 1.7 | --- | 99.1 | IF | 5.28 | 5.52 | 4 |
| | | 3.4 | --- | 99.1 | IF | 5.28 | 4.47 | -15 |

*** IF: Indentation Fracture, SENB: Single Edge Notched Beam**

**Table 1**: Properties of the studied composites

| Material | Relative density (%) | Grain size (μm) | F | Hardness (GPa) | Fracture toughness ($MPa \cdot m^{1/2}$) |
|---|---|---|---|---|---|
| **3YTZP** | 100 | 0.26 ± 0.11 | 0.76 ± 0.06 | 13.0 ± 0.5 | 6.1 ± 0.9 |
| **3YTZP/2.5 vol% SWNT** | 100 | 0.27 ± 0.13 | 0.76 ± 0.06 | 12.4 ± 0.7 | 4.7 ± 0.9 |
| **3YTZP/5 vol% SWNT** | 99.3 | 0.19 ± 0.08 | 0.76 ± 0.07 | 11.4 ± 0.5 | 4.8 ± 0.6 |
| **3YTZP/10 vol% SWNT** | 100 | 0.24 ± 0.13 | 0.76 ± 0.08 | 9.2 ± 0.9 | 5.0 ± 0.8 |

**Table 2**: Comparison of properties for CNT-3YTZP composites reported in literature.

| | Type of CNT | CNT vol% | Grain size (nm) | Relative Density (%) | Method of $K_{IC}$ measurement | $K_{IC}$ (MPa·m$^{1/2}$) | | Relative $K_{IC}$ variation (%) |
|---|---|---|---|---|---|---|---|---|
| | | | | | | Monolithic | Composite | |
| This study | SWNT | 2.5 | 270 | 100 | IF | 6.1 | 4.7 | -23 |
| Shin 2012 (27) | SWNT | 3.4 | 280 | 98.0 | IF | 4.4 | 5.2 | 18 |
| Chintapalli 2012 (24) | MWNT | 2 | 161 | 98.7 | IF | 3.9 | 4.5 | 15 |
| Garmendia 2011 (23) | MWNT | 3 | 218 | 99.5 | IF | 2.36 | 4.06 | 72 |
| | | 6 | 146 | 99.1 | IF | 2.36 | 2.07 | -14 |
| Mazaheri 2011 (9) | MWNT | 12.5 | 96 | 98.4 | IF | 5.5 | 11 | 100 |
| | | | | | SENB | 6 | 8 | 33 |
| Zhou 2009 (25) | MWNT | 3.4 | --- | 98.6 | IF | 4.9 | 5.8 | 21 |
| | | 5 | --- | 98 | IF | 4.9 | 5.2 | 5 |
| Garmendia 2009 | MWNT | 1 | 220 | 95.7 | IF | 3.8 | 4.0 | 5 |
| Duszová 2008 (13) | MWNT | 3.4 | 140 | 88 | IF | 6.24 | 5.6 | -10 |
| Ukai 2006 (11) | MWNT | 1.7 | --- | 100 | IF | 5.56 | 6.10 | 10 |
| | | 3.4 | --- | 100 | IF | 5.56 | 5.69 | 2 |
| Sun 2005 (15) | MWNT | 1.7 | --- | 99.1 | IF | 5.28 | 5.52 | 4 |
| | | 3.4 | --- | 99.1 | IF | 5.28 | 4.47 | -15 |

* IF: Indentation Fracture, SENB: Single Edge Notched Beam

Figure 1

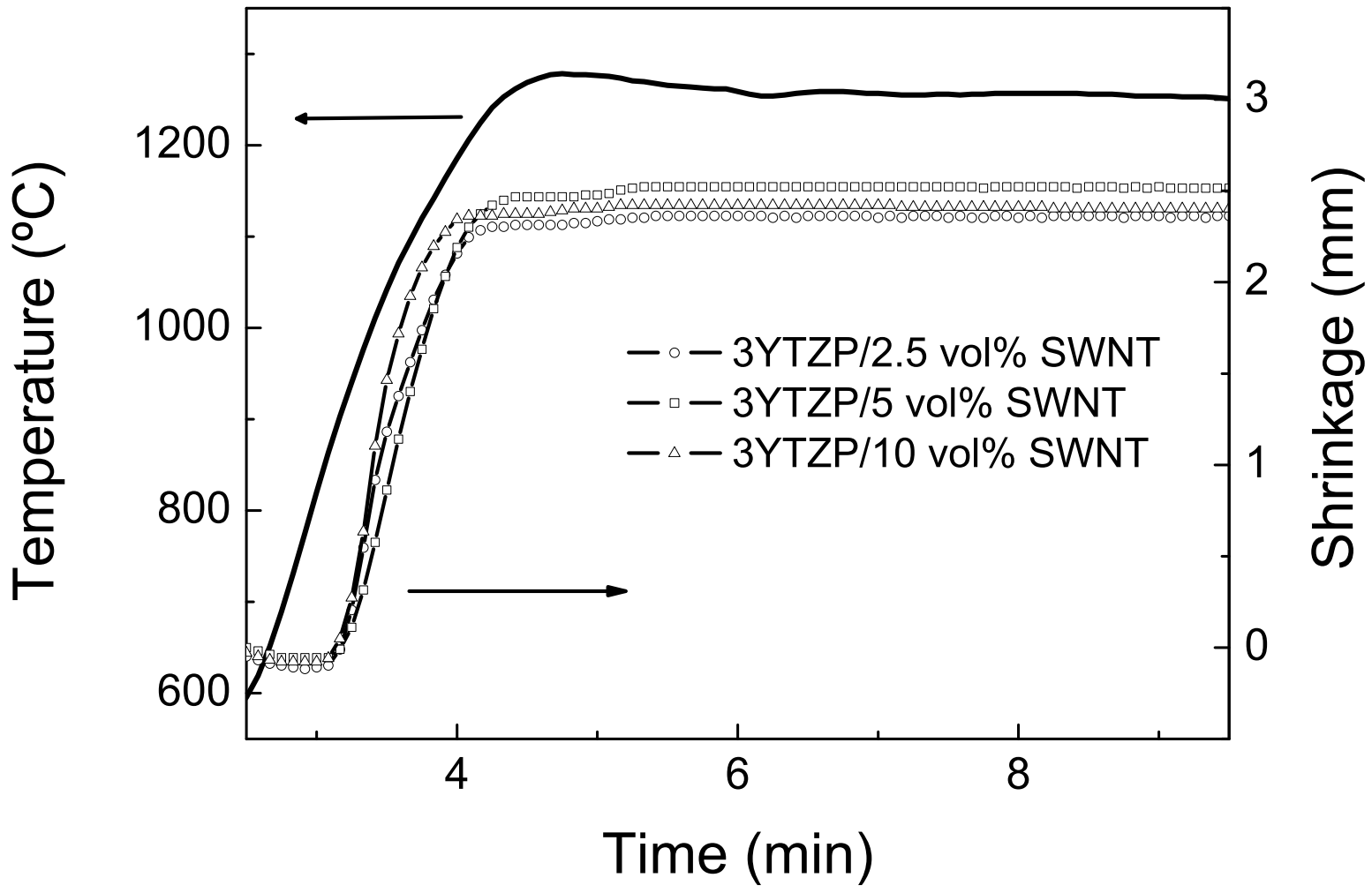
Temperature (ºC)
1200
1000
800
600
4
6
8
Time (min)
3
2
1
0
Shrinkage (mm)
3YTZP/2.5 vol% SWNT
3YTZP/5 vol% SWNT
3YTZP/10 vol% SWNT

Figure 2

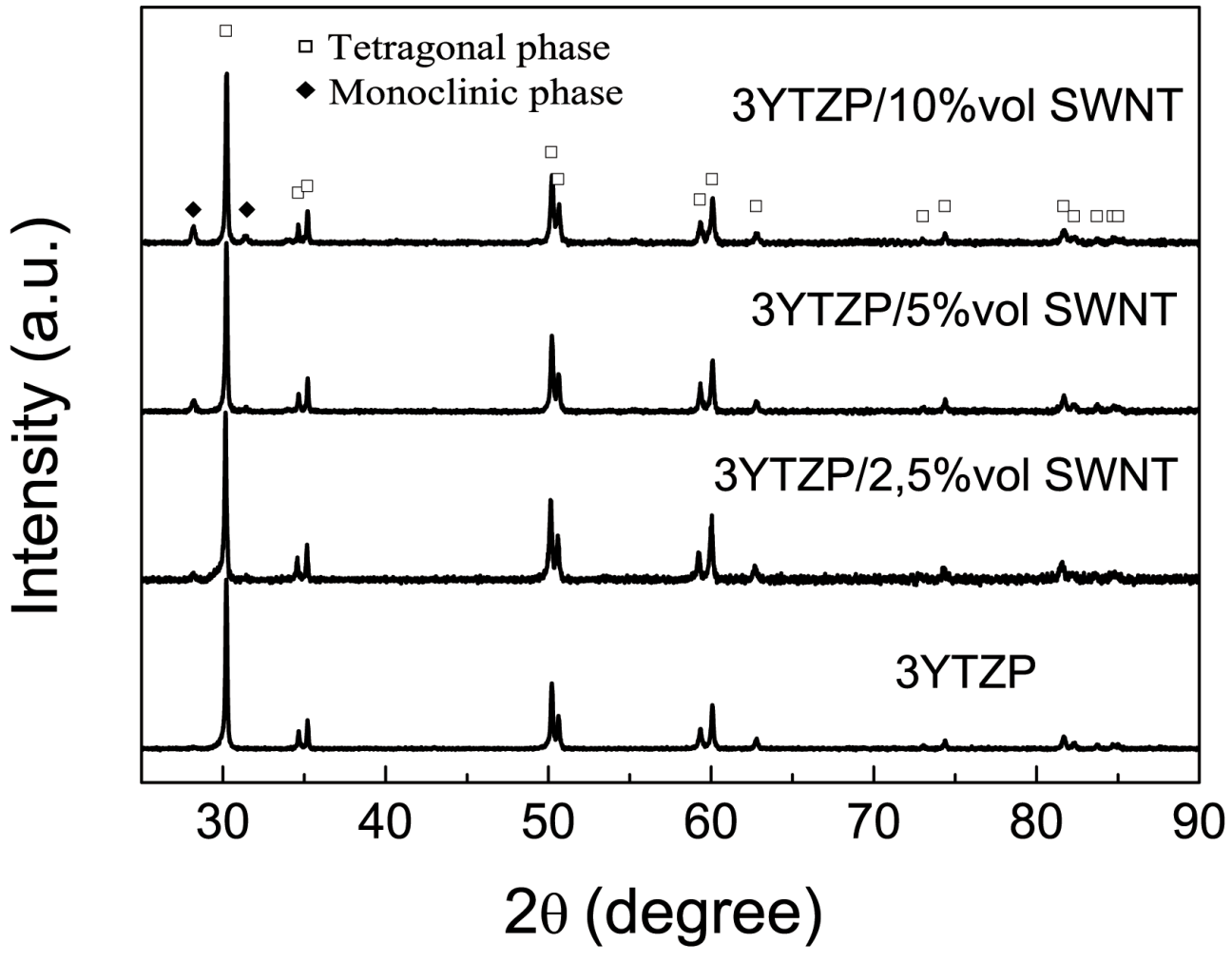
Tetragonal phase
Monoclinic phase
3YTZP/10%vol SWNT
3YTZP/5%vol SWNT
3YTZP/2,5%vol SWNT
3YTZP
Intensity (a.u.)
30
40
50
60
70
80
90
2θ (degree)

Figure 3

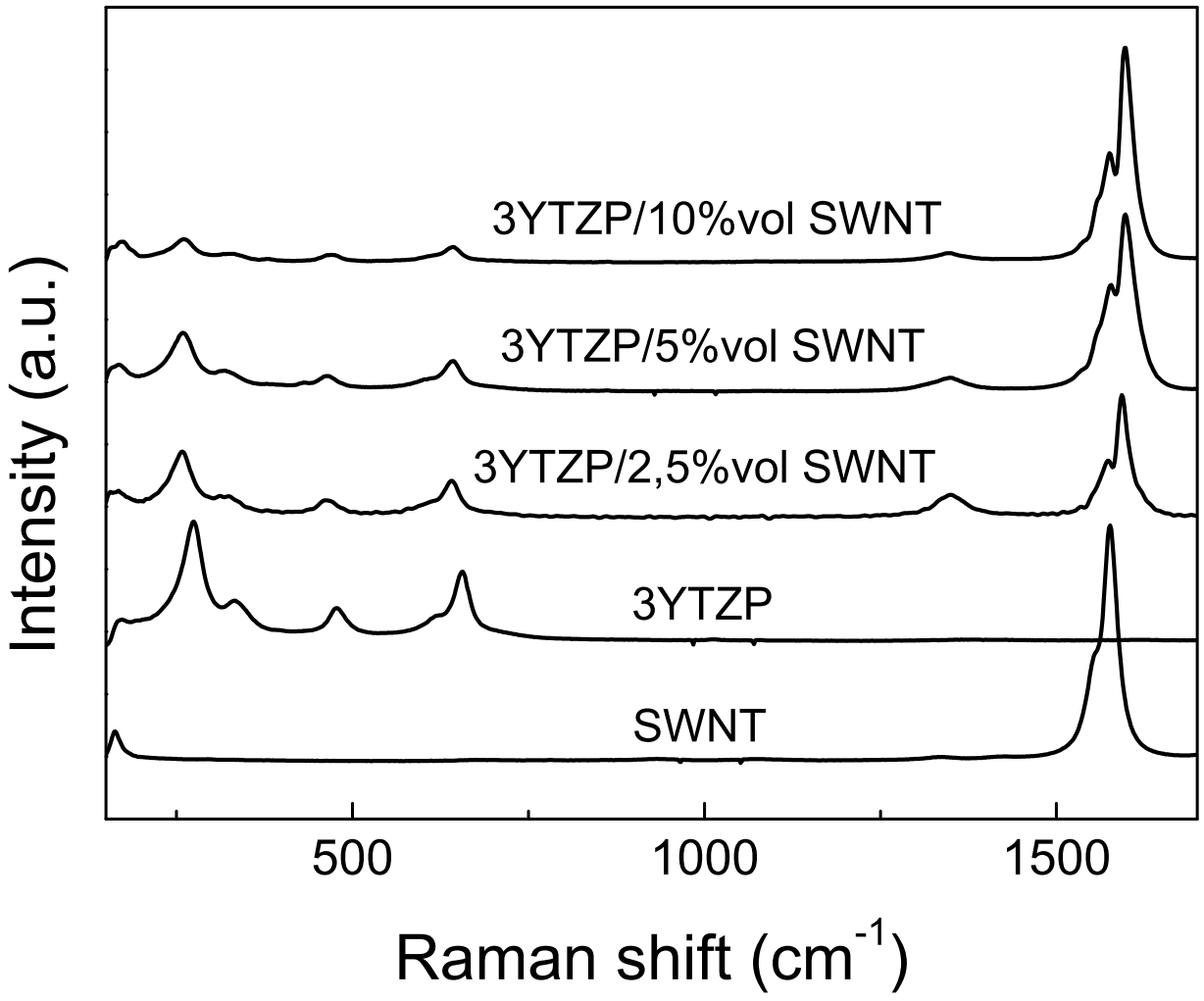
3YTZP/10%vol SWNT
3YTZP/5%vol SWNT
3YTZP/2,5%vol SWNT
3YTZP
SWNT
Intensity (a.u.)
500
1000
1500
Raman shift (cm-1)

**Figure 4**

Click here to download high resolution image

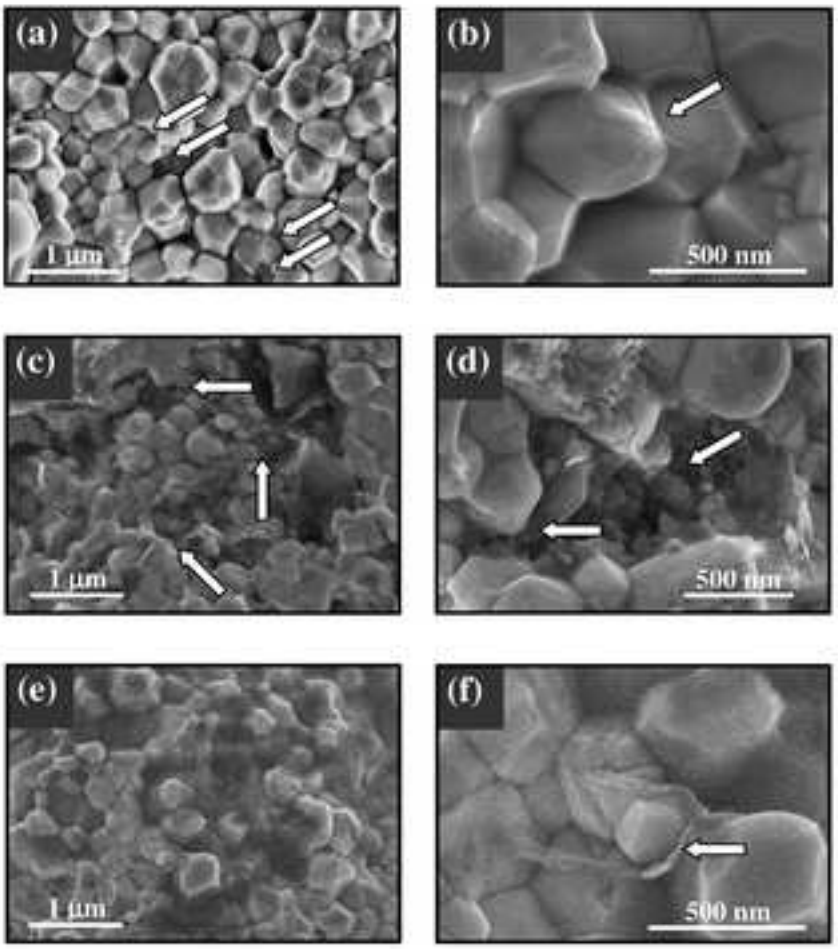

**Figure 5**
**Click here to download high resolution image**

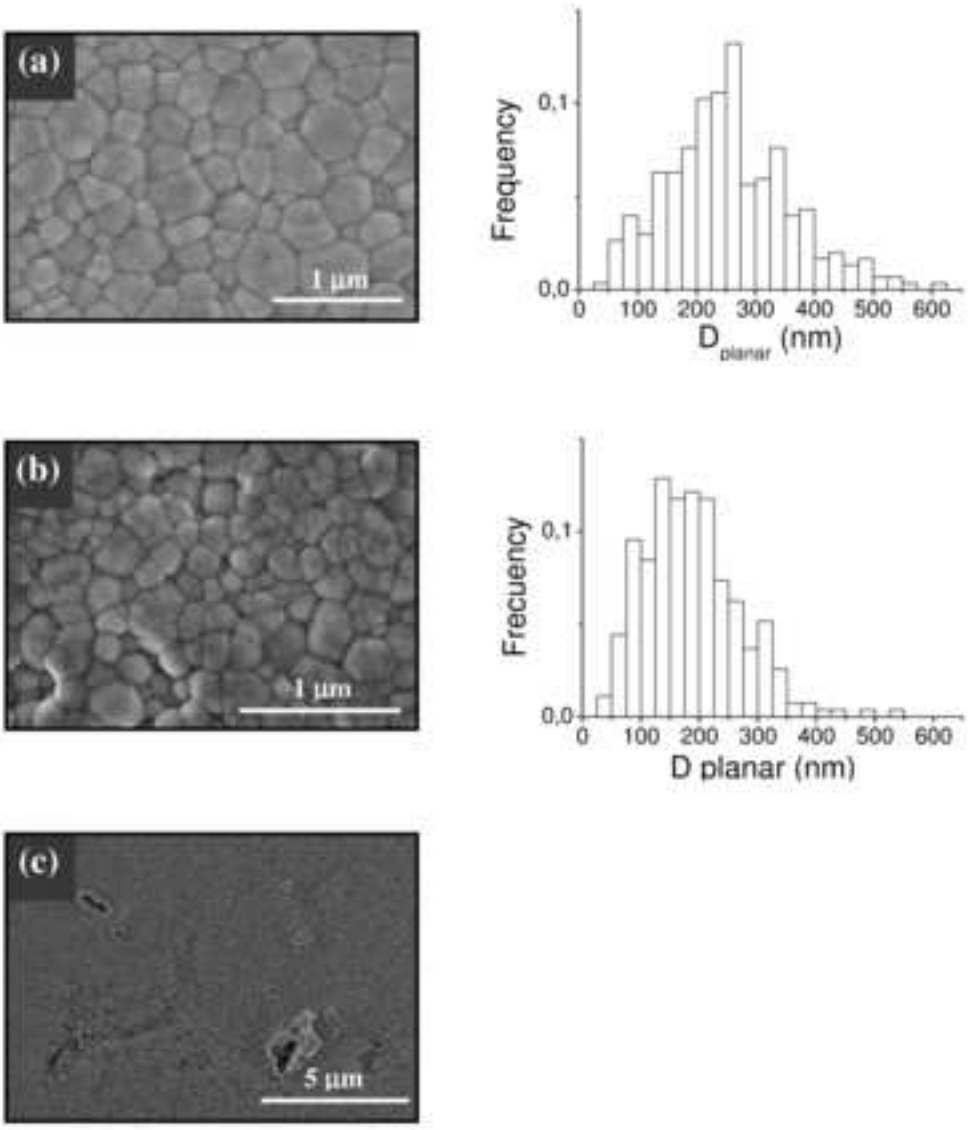


Figure 5

Figure 6

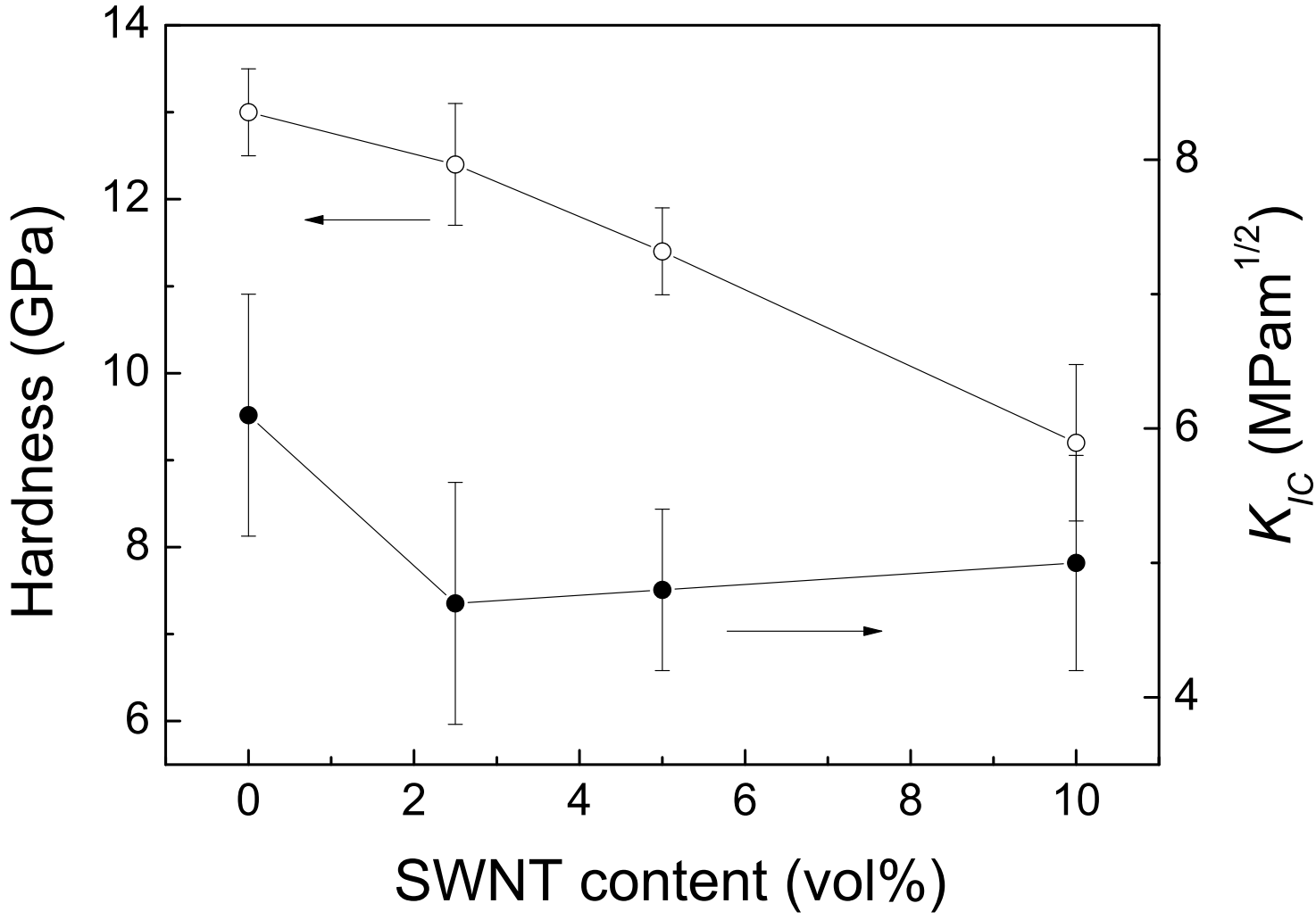
Hardness (GPa)
$K_{IC}$ (MPam$^{1/2}$)
SWNT content (vol%)
14
12
10
8
6
8
6
4
0
2
4
6
8
10

**Figure 7**

**Click here to download high resolution image**

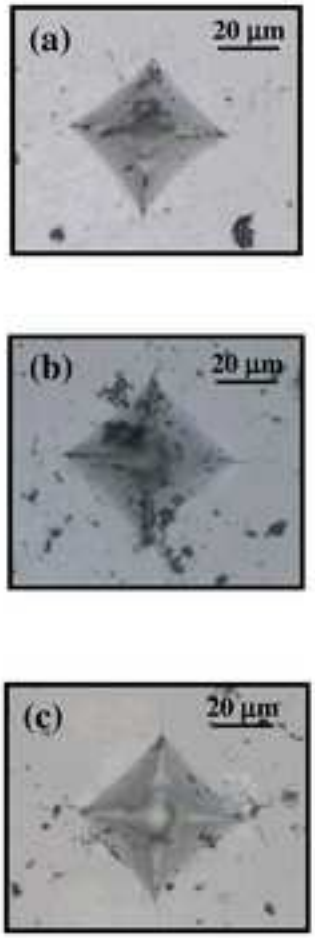

## Figure captions

**Figure 1**: Shrinkage and temperature curves recorded during the SPS processing of the 3YTZP/SWNTs composites.

**Figure 2**: X-ray diffraction patterns of the monolithic 3YTZP ceramic and the composites.

**Figure 3**: Raman spectra measured in the composites including the RBM frequency range, and the D-Band and G-Band frequency range. Raman spectra measured in the monolithic 3YTZP ceramic and in the SWNTs have been included for comparison.

**Figure 4**: HRSEM micrographs of fracture surface of the composites reinforced with different SWNT contents (a) and (b) 2.5 vol%, (c) and (d) 5 vol%, and (e) and (f) 10 vol%.

**Figure 5**: HRSEM micrographs of thermally etched polished surfaces and grain size distribution plots of the (a) monolithic 3YTZP ceramic, and (b) composite reinforced with 5 vol% SWNTs. (c) HRSEM micrographs of thermally etched polished surface of the 3YTZP/5 vol% SWNTs composite, showing some holes related to agglomerates burned out during thermal etching in air.

**Figure 6**: Hardness and indentation fracture toughness of the SWNT-3YTZP composites.

**Figure 7**: SEM micrographs of the Vickers indentations in the composites with (a) 2.5, (b) 5, and (c) 10 vol% SWNTs.